High-throughput rear-surface drilling of microchannels in glass based on electron dynamics control using femtosecond pulse trains

Lan Jiang,[1,*] Pengjun Liu,[1] Xueliang Yan,[1] Ni Leng,[1] Chuancai Xu,[1] Hai Xiao,[2] and Yongfeng Lu[3]

[1]*NanoManufacturing Fundamental Research Joint Laboratory of National Science Foundation of China, School of Mechanical Engineering, Beijing Institute of Technology, 100081, China*

[2]*Department of Electrical and Computer Engineering, Missouri University of Science and Technology, Rolla, Missouri 65409, USA*

[3]*Department of Electrical Engineering, University of Nebraska-Lincoln, Lincoln, Nebraska 68588-0511, USA*

**Corresponding author: jianglan@bit.edu.cn*

Received March 29, 2012; revised May 18, 2012; accepted May 18, 2012; posted May 21, 2012 (Doc. ID 165745); published July 3, 2012

This study proposes a rear-surface ablation enhancement approach to fabricate high-aspect-ratio microchannels by temporally shaping femtosecond laser pulse trains. In the case study of K9 glass, enhancements of up to a 56 times higher material removal rate and a three times greater maximum drilling depth are obtained by the proposed method, as compared with conventional femtosecond laser drilling at the same processing parameters. The improvements are due to the changes of photon-electron interactions by shaping femtosecond pulse train, which can effectively adjust the photon absorption and localized transient material properties by changing electron dynamics such as free electron densities. © 2012 Optical Society of America

OCIS codes: 220.4610, 140.7090.

Recently, fabrication of microchannels has received intensive research interest due to applications in microfluidic devices for liquid or gas, microreactors, and micro total analysis systems. Among materials for the applications, transparent dielectrics, such as silica glass, are particularly attractive, as they exhibit good optical properties in the ultraviolet to infrared wavelength range and excellent chemical/physical stability [1]. Femtosecond lasers are promising tools for the micro/nanoscale ablation of dielectrics with reduced recast, microcracks, and heat-affected zones [2]. In the ablation process, materials are first transformed into absorbing plasma with metallic properties, and then the subsequent laser-plasma interaction causes material removal [3]. Besides, the femtosecond pulse duration is shorter than many physical characteristic times, which makes it possible to manipulate electron dynamics such as excitations, ionizations, recombination, densities, and temperatures of electrons [4,5]. This opens new possibilities for controlling the transient localized material properties and corresponding phase change mechanisms [6,7].

Many researchers have investigated the fabrication of high-aspect-ratio straight and three-dimensional (3D) microchannels using femtosecond lasers [8–13]. Li *et al.* introduced water-assisted, rear-surface microfabrication of 3D holes in silica glass [11]. Hwang *et al.* applied liquid and ultrasonic waves to drill straight and 3D microchannels in glass [12]. Maselli *et al.* reported a process based on the use of an astigmatically shaped beam and chemical etching to fabricate long microchannels with a circular cross section [13]. The previous works have demonstrated the feasibility of femtosecond lasers drilling microchannels, but little attention has been paid to the material removal rate. For transparent dielectric front surface ablation, pulse trains with separation times of nanoseconds or longer can be used to improve the ablation efficiency [14]; however, the ablation depth/volume decreases as the separation time increases from 100 to 1000 fs [15]. Surprisingly, when we focus a femtosecond pulse train with a separation time shorter than 1 ps onto the rear surface of the target, a significant ablation enhancement is obtained, which is a new and interesting phenomenon. We experimentally demonstrated that femtosecond pulse train rear-surface drilling of microchannels in glass is an effective, simple, repeatable throughput method, which does not need any additional steps (such as etching or cleaning) or toxic chemicals.

The schematic diagram of the experimental setup is shown in Fig. 1(a). The laser used in the experiment is a commercial chirped Ti: sapphire regenerative oscillator-amplifier system (Spectra-Physics). The femtosecond laser pulse is linearly polarized, with a central wavelength of 800 nm, pulse width of 50 fs (FWHM) and repetition rate of 1 KHz.

By combining a half-wave plate with a polarizer, the pulse energy can be continuously varied. The

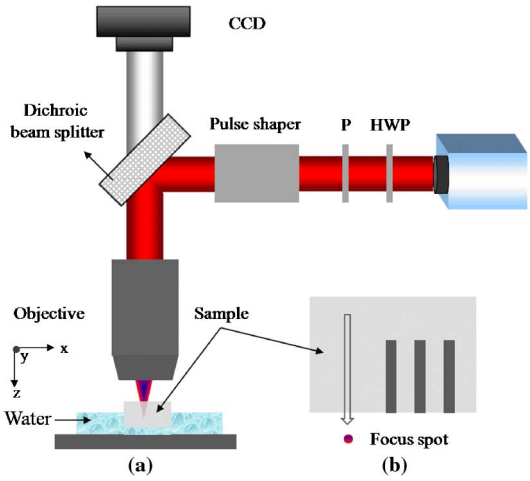

Fig. 1. (Color online) Schematic diagram of (a) the experimental setup for fabrication of microchannels and (b) the partial enlarged view in the sample. P, polarizer; HWP, half-wave plate.

femtosecond laser pulse is temporally shaped to be a pulse train with an accurate pulse delay, nearly equal energy distribution, and an identical pulse duration between the subpulses by a pulse shaper (BSI MIIPS BOX 640), which is from Biophotonic Solutions Inc. A 640 pixel liquid crystal spatial light modulator is inserted in the Fourier plane of a zero-dispersion stretcher; the detailed principle of pulse shaping is explained by Weiner [16]. A 1.5 mm thick, all-surfaces polished sample (K9 glass) is mounted in a glass dish filled with distilled water. The sample bottom is immersed in water to reduce the blocking and redeposition effects of ablated debris. The glass dish is mounted on a six-axis piezo stage with positioning accuracy of 1 μm in the x and y directions and 0.5 μm in the z direction. The laser beam propagates along the $+z$ direction and is focused by a 0.3 N.A. microscope objective. The pulse trains used in experiments consist of two subpulses, and the pulse delays range from 0 to 1000 fs (a double pulse per train with 0 fs delay is actually a conventional pulse). At the beginning, the laser beam is focused on the rear surface of the glass; and then the sample is moved along the $-z$ direction by 50 μm to guarantee that the focused spot is beneath the rear surface, as shown in Fig. 1(b). The piezo stage is programmed to move along the $+z$ direction with a preset constant speed until termination, and microchannels are fabricated in a single step.

Figure 2(a) shows the microchannels drilled in K9 glass by conventional femtosecond pulse of 20 μJ at a 1 KHz repetition rate. At a processing speed of 2 μm/s, the drilling depth is about 150 μm, and the material removal rate is 0.5 μm^3/pulse (assuming cylindrical microchannels). When the processing speed is increased, the drilling depth rapidly drops down to less than 10 μm. In contrast, at the same total energy, deeper microchannels can be fabricated by the proposed pulse train method, as shown in Fig. 2(b), in which the two subpulses are equally distributed in energy with a pulse delay of 500 fs. The maximum material removal rate reaches up to 28 μm^3/pulse, which is 56 times higher than that by conventional femtosecond laser drilling at the same total energy. It is worth noting that the ablated debris cannot be drained out effectively as the depth increases, which limits the microchannel depth eventually [12].

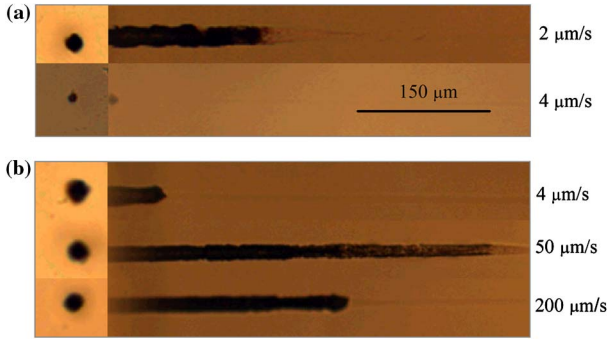

Fig. 2. (Color online) Microscopic cross-sectional and entrance opening images of microchannels drilled in contact with distilled water by (a) conventional pulse and (b) pulse train of 20 μJ at a 1 KHz repetition frequency.

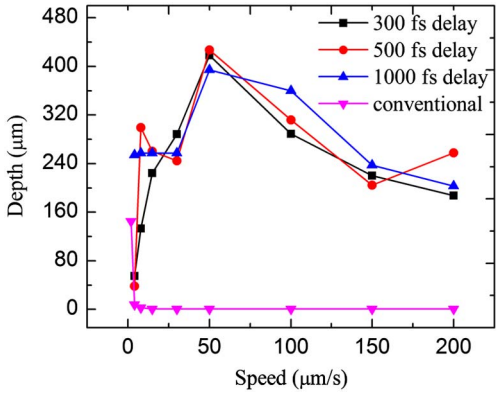

Fig. 3. (Color online) Plot of microchannel depths against processing speed of a pulse train and conventional pulse at 20 μJ, 1 KHz repetition frequency.

Figure 3 shows the plot of microchannel depths versus processing speed of a pulse train and a conventional femtosecond pulse at 20 μJ, 1 KHz repetition rate. Each point in Fig. 3 represents an average of three experimental data points with a standard deviation of 8–12%. The error bars of the standard deviation are not shown for clarity. For femtosecond pulse train drilling, the drilling depth is small when the processing speed is low (4 μm/s). This may be due to excessive energy deposition that destroys the lattice near the laser focus, which diffracts the laser beam. Drilling depth increases with a processing speed in the range of 4–50 μm/s. When the processing speed is 50 μm/s, the drilling depth reaches maximum (~450 μm), which is about three times greater than the maximum depth (~150 μm) drilled by a conventional femtosecond laser at the same energy. When the processing speed is higher (>50 μm/s), the drilling depth begins to drop down due to the reduction of photon energy deposited per unit of time. Although the drilling depths by pulse trains with different pulse delays are similar, the drilling morphologies, which are not presented in this paper, are somewhat different.

As shown in Fig. 4, the entrance diameters drop down dramatically as the processing speed increases, for conventional femtosecond laser drilling, while the entrance diameters drop down slowly for fs pulse train drilling.

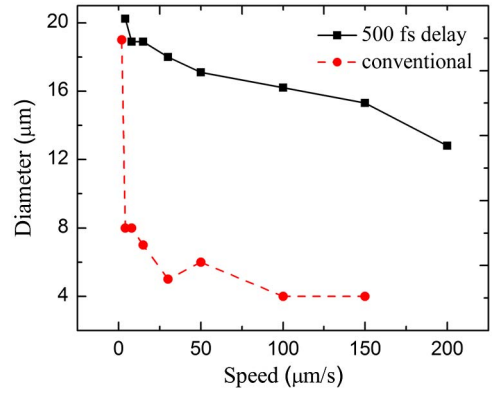

Fig. 4. (Color online) Plot of microchannel entrance diameters against processing speed of a pulse train and conventional pulse at 20 μJ, 1 KHz repetition frequency.

Fig. 5. (Color online) Microscopic cross-sectional images of microchannels drilled in contact with distilled water by a pulse train of 35 μJ with a pulse delay of 800 fs at 1 KHz repetition frequency.

For clarity, only the results of a 500 fs delayed pulse train are plotted; other cases of pulse trains at different delays are similar. Figure 5 shows the maximum aspect ratio of microchannels (~40:1) fabricated in K9 glass at an energy of 35 μJ, processing speed of 80 μm/s, and pulse delay of 800 fs. The two microchannels shown in Fig. 5 were fabricated under the same processing parameters, and the difference in depth and morphology might result from pulse energy fluctuations. Figure 6 shows the scanning electron microscopy (SEM) images of rear surface ablation in a single shot with an energy of 2 μJ. The laser beam is focused on the rear surface of the sample. It is obvious that the ablation volume of the pulse train (500 fs pulse delay) is much greater than that by the conventional femtosecond pulse. Filament [17] may occur in experiments. Yet, no detailed study has been done in this regard.

The experimental results indicate that the photon absorption efficiency of a pulse train is much higher than that by the conventional femtosecond laser in the rear-surface ablation process. The photon absorption efficiency enhancement is due to the change in the free electron density distribution by the pulse train technology. In our previous work, a plasma model was proposed for ultrashort pulse laser ablation of dielectrics to investigate free electron generation and distribution [3]. At the same total fluence, for conventional femtosecond pulse laser processing of the sample, after critical electron density is achieved by nonlinear ionization (photoionization and impact ionization), the reflectivity of the ionized zone increases rapidly, and the subsequent laser energy is significantly reflected, which leads to the lower photon absorption efficiency. However, at the lower fluence of an individual subpulse for a pulse train, fewer free electrons are generated and the reflectivity is lower. Thus, more laser energy is absorbed using the pulse train technology.

In summary, a high throughput method for enhancement of the material removal rate in rear surface ablation has been demonstrated by temporally shaping a femtosecond pulse train. By focusing the pulse train laser beam onto the rear surface of the K9 glass, the temporal and spatial electron density distributions are manipulated by the pulse train shaping, which increases the photon absorption efficiency. For the process conditions in this study, it is shown that the material removal rate and the maximum drilling depth are enhanced by about 56 times and three times, respectively, by employing the proposed method, as compared with conventional femtosecond laser drilling at the same processing parameters,

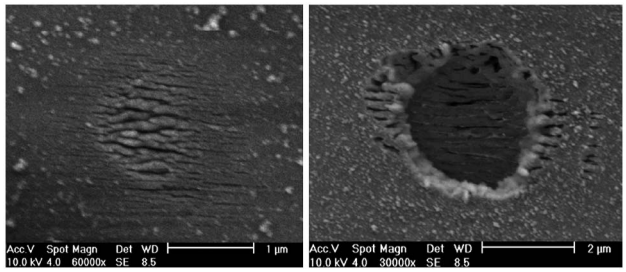

Fig. 6. SEM images of rear surface ablation in a single shot with a pulse energy of 2 μJ conventional pulse (left) versus a pulse train with a delay of 500 fs (right).

including the total energy, wavelength, and so on. Detailed experiments should be conducted to investigate the mechanisms during femtosecond pulse train ablation. In addition, nonlinear phenomenon, such as temporal/spatial splitting and self-focusing/defocusing, should also be considered to further improve the performance of pulse train processing based on the electron dynamics control mechanism.

This research is supported by the National Basic Research Program of China (973 Program) (grant 2011CB013000) and National Natural Science Foundation of China (NSFC) (grants 90923039 and 51025521).

References

1. A. Said, M. Dugan, and P. Bado, Opt. Express **12**, 2120 (2004).
2. C. H. Lin, Z. H. Rao, L. Jiang, W. J. Tsai, P. H. Wu, C. W. Chien, S. J. Chen, and H. L. Tsai, Opt. Lett. **35**, 2490 (2010).
3. L. Jiang and H. L. Tsai, J. Appl. Phys. **100**, 023116 (2006).
4. E. Goulielmakis, V. S. Yakovlev, A. L. Cavalieri, M. Uiberacker, V. Pervak, A. Apolonski, R. Kienberger, U. Kleineberg, and F. Krausz, Science **317**, 769 (2007).
5. C. Wang, L. Jiang, F. Wang, X. Li, Y. P. Yuan, and H. L. Tsai, Phys. Lett. A **375**, 3200 (2011).
6. S. X. Hu and L. A. Collins, Phys. Rev. Lett. **96**, 073004 (2006).
7. F. Remacle and R. D. Levine, Proc. Natl. Acad. Sci. USA **103**, 6793 (2006).
8. Y. Li, S. L. Qu, and Z. Y. Guo, J. Micromech. Microeng. **21**, 075008 (2011).
9. Y. Li and S. L. Qu, Mater. Lett. **64**, 1427 (2010).
10. F. He, H. Xu, Y. Cheng, J. Ni, H. Xiong, Z. Xu, K. Sugioka, and K. Midorikawa, Opt. Lett. **35**, 282 (2010).
11. Y. Li, K. Itoh, W. Watanabe, K. Yamada, D. Kuroda, J. Nishii, and Y. Jiang, Opt. Lett. **26**, 1912 (2001).
12. D. J. Hwang, T. Y. Choi, and C. P. Grigoropoulos, Appl. Phys. A **79**, 605 (2004).
13. V. Maselli, R. Osellame, G. Cerullo, R. Ramponi, P. Laporta, L. Magagnin, and P. L. Cavallotti, Appl. Phys. Lett. **88**, 191107 (2006).
14. D. Esser, S. Rezaei, J. Z. Li, P. R. Herman, and J. Gottmann, Opt. Express **19**, 25632 (2011).
15. I. H. Chowdhury, X. Xu, and A. M. Weiner, Appl. Phys. Lett. **86**, 151110 (2005).
16. A. M. Weiner, Rev. Sci. Instrum. **71**, 1929 (2000).
17. X. L. Mao, S. S. Mao, and R. E. Russo, Appl. Phys. Lett. **82**, 697 (2003).